Ball milling synthesis and BCC to FCC phase transition under pressure in nanostructured NANOPERM alloys

V. D. COJOCARU[*], F. TURQUIER[a], R. NICULA[a], M. STIR[a], E. BURKEL[a]
Politehnica University of Bucharest, Spl. Independentei 313, 060042 Bucharest, Romania
[a]*University of Rostock, Physics Department, August-Bebel-Str. 55, D-18055, Rostock, Germany.*

The main aim of the present work is to study the synthesis and stability of soft-magnetic nanostructured materials under high pressure – high temperature conditions. NANOPERM alloy powders were prepared by high-energy ball-milling. The as-milled alloys consist of a iron-based nanocrystalline solid solution. The evolution of crystallinity and grain-size during the ball-milling process and investigations under external pressure up to 3 GPa for temperatures up to 1200°C were evaluated using synchrotron radiation X-ray diffraction. The X-ray experiments were performed at the B2/MAX80 instrument beamlines at DESY/HASYLAB, Hamburg, Germany.

1. Introduction

Amorphous and more recently nanocrystalline materials were investigated for applications in magnetic devices such as transformers, inductive devices, etc, which use soft-magnetic materials. The interest in developing nanocrystalline soft-magnetic alloys has dramatically increased during the past few years.

Bulk soft-magnetic materials need to have both high induction and permeability, as well as many non-magnetic issues such as mechanical properties, corrosion resistance, etc. Key issues include alloy chemistry, structure and the ability to tailor microstructural features. Nanocrystalline magnets used in soft magnetic applications must therefore be optimised in terms of intrinsic and extrinsic magnetic properties as well as their morphology [1].

The key intrinsic magnetic properties, the saturation magnetic induction (Bs), the Curie temperature (T_C), are determined by the alloy composition and crystal structure. The extrinsic property of interest are the magnetic permeability (μ) and the magnetic response function in an applied field, which usually is inverse related to the coercivity (H_C) of the magnetic material. In particular, alloys with small magnetocrystalline anisotropy and magnetostrictive coefficients give rise to improved soft magnetic materials [2].

2. Experimental procedure

Nanocrystalline powder precursors for the soft magnetic alloy $Fe_{88}Zr_7B_4Cu_1$ (NANOPERM) were obtained by high-energy ball-milling (RETSCH 400 PM planetary ball-mill) from high-purity elemental powders with an average particle-size close to 100 μm.

The elemental powders were immersed in hexane and mechanically milled in stainless steel vials (250 ml) with stainless steel balls (20 mm diameter) at 250 rotations per minute (rpm). The ball-to-powder mass ratio was 20:1 and the total milling time was 90 hours. The resulting milling parameters were as follows: impact energy E = 0.1378 Joule and milling intensity I = 2.4806 Watt [3]. During milling, small quantities of powder were taken out for further investigations. The grain-size evolution during milling was investigated at the high-resolution powder diffractometer instrument B2 beamline from DESY/HASYLAB (Hamburg, Germany).

Morphological observation upon ball-milled powder was made using a scanning electron microscope TESCAN VEGA II – XMU.

The thermal stability of ball-milled powder precursors was also investigated under high-pressure - high-temperature conditions, using applied pressures up to 3 GPa and temperatures up to 1200 ^{0}C. The experiments were performed in EDX mode at the multiple-anvil high-pressure instrument MAX80 at DESY/HASYLAB (Hamburg, Germany).

3. Results

3.1. Grain-size evolution during milling

The grain-size evolution of during the ball-milling process was obtained from synchrotron radiation X-ray diffraction experiments.

The evolution of X-ray diffraction patterns is presented in figure 1, where the bcc-α(110), bcc-α(200) and bcc-α(211) peaks of Fe are shown. The diffraction patterns were fitted using the PeakFit v4.11 software package (SYSTAT Software Inc.). The Fe diffraction

peaks suffer changes during milling, i.e., the peaks intensities decrease and the full-width-at-half-maximum (FWHM) parameter increases, during milling, meaning that the average dimensions of crystalline domains become smaller.
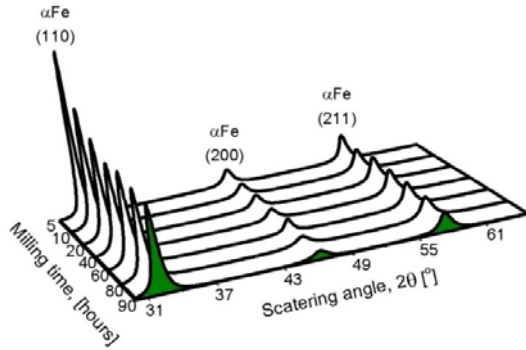

Fig. 1. Powder diffraction spectra evolution during milling.

The calculated values for the grain-size evolution are presented in the Fig. 2 and Fig. 3. Fig. 2 illustrates the evolution of dimensions of crystalline domains as obtained from the FWHM of the bcc-αFe (110) peak, using the Scherrer equation (equation 1) [4]:

$$\beta \cdot \cos\theta = \frac{k \cdot \lambda}{D} \quad \text{(Scherrer)} \qquad (1)$$

where β is the pure broadening of the diffraction peak measured at half the maximum intensity (FWHM parameter), θ the Bragg angle, k the shape factor (k = 0.9), λ = 0.1135 nm is the wavelength of the X-ray radiation, and *D* the average dimension of crystallites (grain-size).
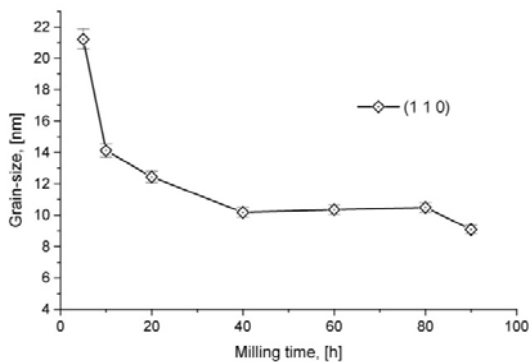

Fig. 2. Grain-size evolution during milling using Scherrer equation (the line is a guide to the eye).

Fig. 3 illustrates the evolution of grain-size and the average internal microstrain. If the internal microstrain is considered than equation 1 can be rewritten as [4]:

$$\beta \cdot \cos\theta = 2 \cdot \varepsilon \cdot \sin\theta + 0{,}9 \cdot \frac{\lambda}{D} \text{(Williamson-Hall)} \qquad (2)$$

where ε is the average microstrain.

The grain-size evolution during milling is as follows: after 5 hours milling time the value of grain-size is equal to 21 nm if internal microstrains are ignored and 27 nm if the influence of internal microstrains is taken into account. At the end of the milling process the grain-size equals 9 nm (Scherrer) or 13 nm if the Williamson-Hall procedure (equation 2) is used.
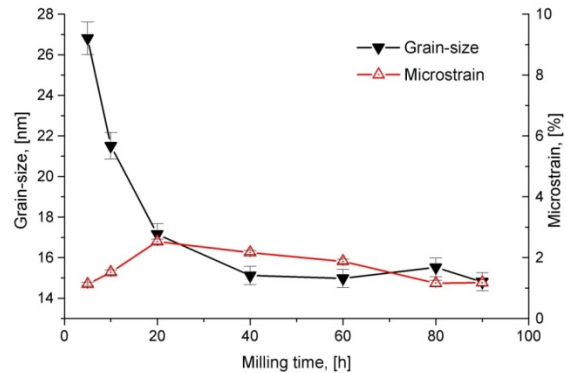

Fig. 3. Grain-size and internal strain evolution during milling (the lines are guides to the eye).

The internal strain shows a small increase in the initial part of the milling process (up to 2 % after 20 hours of milling). The microstrain decreases to approx. 1 % towards the end of the milling process. It was also observed that the grain-size decreases with milling time up a critical grain-size of about 15 nm. For milling times beyond 40 hours the grain-size reduction process stops.

3.2. Particle-size evolution during milling

As observed in Fig. 4 – 8 one can see that for short milling time, see fig. 4, placketar (flakes like) layered particles are formed. Average particle (flakes) size is situated to approx. 25 μm. A small fraction of particles with small dimensions are present.
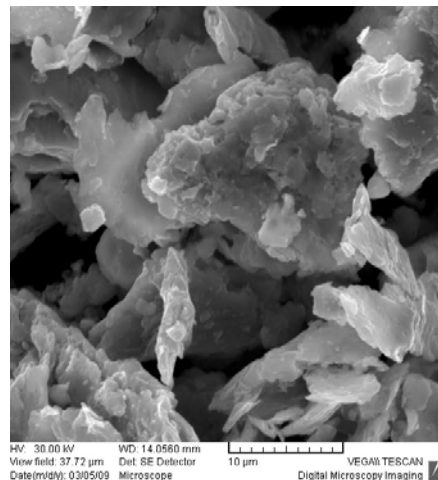

Fig. 4. SEM image for 5 hours milled powder.

Increasing the milling time to 10 hours, see fig. 5, general placketar layered particle shape is maintained, a large decreasing in average flakes size is observed. Average particle size is situated to approx. 12 μm. The fraction of smaller size particles, presented on particle surfaces, is increasing.

For 20 hours milling time, see fig. 6, a decreasing in average particle size is observed. Average particle (flakes) size is situated to approx. 7 μm. The fraction of smaller size particles, presented on large particle surfaces, is increasing also.
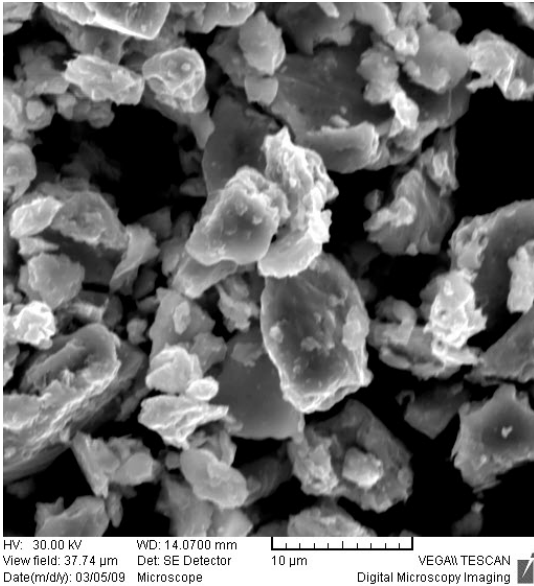

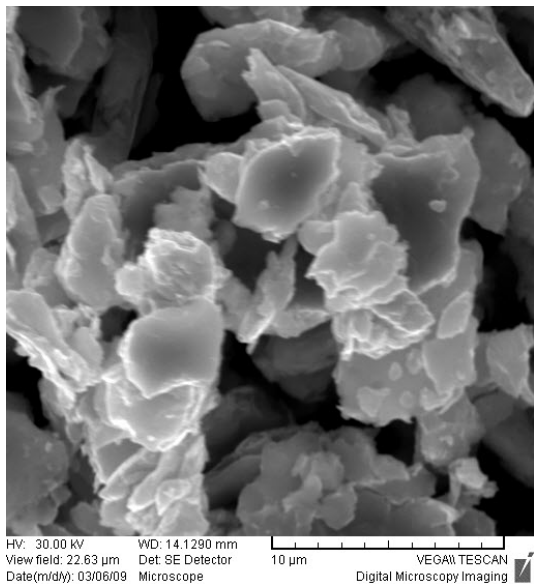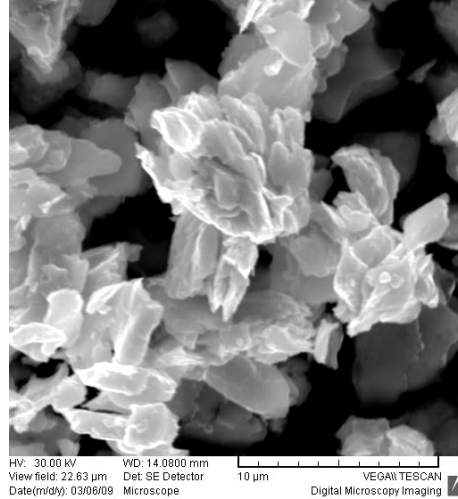*Fig. 5. SEM image for 10 hours milled powder.*

Fig. 7. SEM image for 40 hours milled powder.

For 40 hours milling time, see fig. 7, also a decreasing in average particle size is present. Average particle size is situated to approx. 5 μm. Aglomerated particles are observed.

For 60 hours milling time, see fig. 8, an uniformisation in particles distribution is observed, due to the high intensity particle fragmentation during higher milling times. Average particle size is situated to approx. 5 μm.
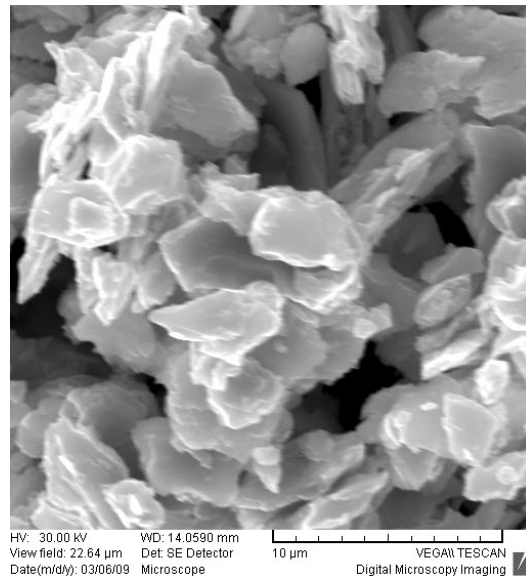

Fig. 8. SEM image for 60 hours milled powder.

3.3. Differential Scanning Calorimetry

Differential scanning calorimetry (DSC) was used to investigate the phase transitions taking place in

Fig. 6. SEM image for 20 hours milled powder.

nanocrystalline NANOPERM alloys. A high-temperature NETZSCH – Pegasus 404C calorimeter was employed. The heating and cooling scans were performed in vacuum at a heating rate equal to 20 K/min. Figure 9 presents the DSC trace for NANOPERM alloy powders.
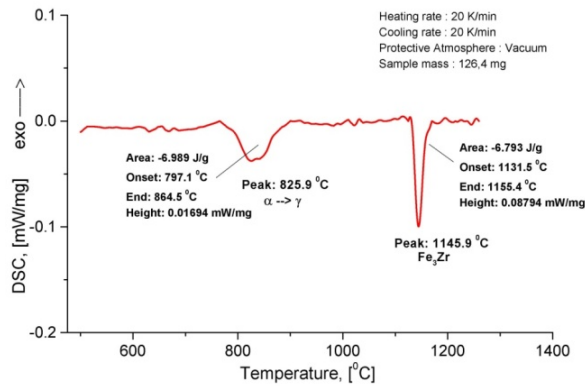

Fig. 9. DSC trace for NANOPERM alloy powders.

The endothermal reaction observed at 826°C represents the transition from the low-temperature stable α-Fe (BCC - phase) to the high-temperature stable phase, γ-Fe (FCC). The $\alpha \rightarrow \gamma$ transition has its onset temperature at 797 ^{0}C and end temperature at 864 ^{0}C. The second endothermal event at 1146 ^{0}C corresponds to the formation of the Fe_3Zr compound.

3.4. BCC to FCC phase transition under pressure

A series of high-pressure X-ray diffraction experiments were performed in energy dispersive mode at the follow pressures: ambient pressure, 0.762 GPa, 1.023 GPa, 1.410 GPa, 1.713 GPa, 2.333 GPa and 2.741 GPa. Heating up to 1200 ^{0}C followed by quenching under pressure were performed at each of the above pressures.
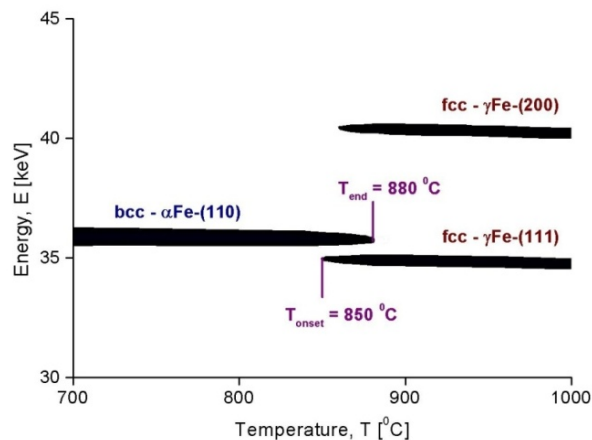

Fig. 10. In-situ $\alpha \rightarrow \gamma$ transition as a function of temperature at 2.741 GPa applied pressure.

Fig. 10 shows a two-dimensional map of the scattered intensity as a function of temperature for a pressure-assisted experiment at 2.741 GPa. The onset of the $\alpha \rightarrow \gamma$ transition is noticed at 850°C, as indicated by the first observation of the γ (111) and (200) diffraction lines (Fig. 10). The end of the $\alpha \rightarrow \gamma$ transformation is marked by the dissapearance of the α (110) diffraction line at 880°C.
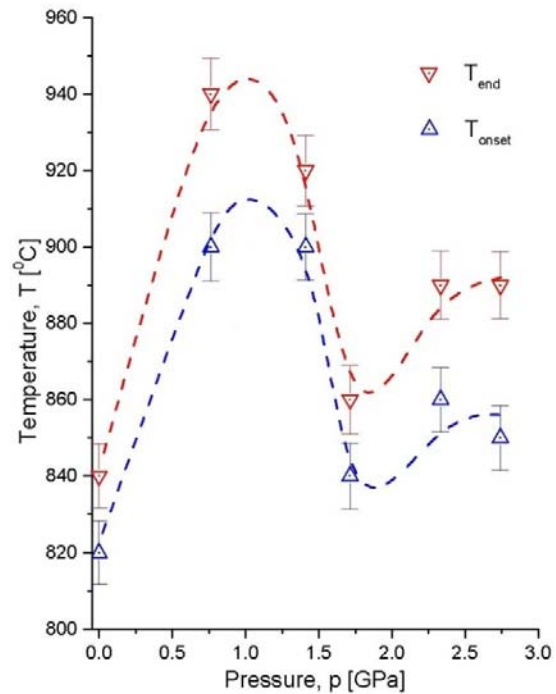

Fig. 11. The influence of external pressure on the $\alpha \rightarrow \gamma$ transition temperatures (dotted lines are guides to the eye).

The onset and end temperatures of the $\alpha \rightarrow \gamma$ (BCC to FCC) phase transition in NANOPERM alloys are plotted as a function of applied pressure in Fig. 11.

The pressure – temperature diagram in Fig. 11 may be divided into three regions:

I - includes the pressure range up to 1.00 GPa: the onset and end of the $\alpha \rightarrow \gamma$ transition are shifted to higher temperature values with increasing pressure. And overall increase of about 100°C in both transition temperatures is reached at pressures close to 1 GPa.

II - corresponds to pressures between 1.00 – 1.75 GPa: the onset and end temperatures of the $\alpha \rightarrow \gamma$ transition decrease with increasing pressure, contrary to the behaviour observed within Region I. A minimum is reached at pressure values close to 1.75 GPa ($T_{onset} = 840°C$, $T_{end} = 860°C$).

III - for pressures above p = 1.75 GPa, the $\alpha \rightarrow \gamma$ transition temperatures re-start to increase with the applied pressure, however at a reduced rate compared to Region I (only about 25°C/GPa compared to 120°C/GPa for Region I).

4. Discussion

A tentative explanation of the observed influence of pressure onto the $\alpha \rightarrow \gamma$ phase transition temperatures should rely on the dependence of the homogeneous nucleation rate on both the nucleation barrier and the activation energy for diffusion (equation 3) [5]:

$$I = I_0 \cdot \exp\left(-\frac{\Delta G^* + Q}{k_B \cdot T} \right) \qquad (3)$$

where ΔG^* is the free energy required to form one nucleus of the new phase, Q is the activation energy for diffusion and k_B is the Boltzmann constant. The occurrence of extreme points (maxima or minima) in the pressure dependence of the transition temperatures then results from the competition between ΔG^* and Q and their evolution with external pressure [6-8].

5. Conclusions

In-situ high-pressure – high-temperature synchrotron radiation diffraction experiments were performed in the low pressure range below 3 GPa in order to gain a deeper understanding on the influence of applied pressure on the BCC-to-FCC ($\alpha \rightarrow \gamma$) transition in NANOPERM alloys. Three distinct regions could be evidenced for the dependence of transition temperatures as a function of applied pressure. Work is in progress to quantitatively describe the observed behaviour in terms of competing effects related to the pressure variation of the energy barrier for the nucleation of the FCC γ-phase (within the α-phase BCC matrix) and the activation energy for diffusion, respectively.

References

[1] M. E. McHenry, M. A. Willard, D. E. Laughlin, Progress in Material Science, **44**, 291 (1999).
[2] M. E. McHenry, M. A. Willard, H. Iwanabe, R. A. Sutton, Z. Turgut, A. Hsiao, D. E. Laughlin, Bulletin of Material Science **22**, 495 (1999).
[3] V. D. Cojocaru, Metalurgia International **10**(2), 11 (2005).
[4] J. He, F. Zhou, G. Chang, E. J. Lavernia, Journal of Materials Science, **36**, 2955 (2001).
[5] F. Ye, K. Lu, Phyical Review B **60**, 7018 (2000).
[6] Y. X. Zhuang, J. Z. Jiang, T. J. Zhou, H. Rasmussen, L. Gerward, M. Mezouar, W. Crichton, A. Inoue, Applied Physics Letters, **77**, 4133 (2000).
[7] J. Z. Jiang, T. J. Zhou, H. Rasmussen, U. Kuhn, J. Eckert, C. Lathe, Applied Physics Letters **77**, 3553 (2000).
[8] J. Z. Jiang, J. S. Olsen, L. Gerward, S. Abdali, J. Eckert, N. Schlorke-de Boer, L. Schultz, J. Truckenbrodt, P. X. Shi, Journal of Applied Physics, **87**, 2664 (2000).

_____
[*]Corresponding author: dan.cojocaru@mdef.pub.ro